2011 50th IEEE Conference on Decision and Control and
European Control Conference (CDC-ECC)
Orlando, FL, USA, December 12-15, 2011

# Vision-based Local-level Frame Mapping and Planning in Spherical Coordinates for Miniature Air Vehicles

Huili Yu* Randal W. Beard**

*Abstract*—**This paper presents a vision-based collision avoidance technique for Miniature Air Vehicles (MAVs) using local-level frame mapping and planning in spherical coordinates. To explicitly address the obstacle initialization problem, the maps are parameterized using the inverse time-to-collision (TTC), which is independent of the ground speed of the MAV. Using bearing-only measurements, an extended Kalman Filter (EKF) is employed to estimate the inverse TTC, azimuth, and elevation to obstacles. A nonlinear observability analysis is used to derive conditions for the observability of the system. Based on these conditions, we design a path planning algorithm that minimizes the estimation uncertainties while simultaneously avoiding collisions with obstacles. The behavior of the planning algorithm is analyzed and the characteristics of the environment in which the planning algorithm guarantees collision-free paths for MAVs are described. Numerical results show that the proposed method is successful in solving the path planning problem for MAVs.**

## I. Introduction

Miniature Air Vehicles (MAVs) have the potential to perform tasks that are too difficult or dangerous for human pilots. For example, they can monitor critical infrastructure and disasters, perform search and rescue, and perform in-storm weather measurements [1]. For many of these applications, MAVs are required to navigate in urban or unknown terrains where obstacles of various types and sizes may hinder the success of the mission. MAVs must have the capability to autonomously plan paths that do not collide with buildings, trees, or other obstacles. Therefore, the path planning problem for MAVs has received significant attention [1]–[5].

The general framework for the path planning problem can be described as follows: given a description of the environment, find a feasible path between two configurations in the environment that does not result in collisions with any of obstacles. The path planning problem can be grouped into global path planning and local path planning. Global path planning requires complete knowledge of the environment and a static terrain. In that setting a feasible path from the start to the destination configuration is generated before the vehicle begins its motion [6]. The global path planning problem has been addressed by many researchers and common solution techniques include potential fields methods, probabilistic roadmap methods, and cell decomposition methods [7].

*Graduate research assistant in the Department of Electrical and Computer Engineering, Brigham Young University, Provo, USA, huiliyu.yhl@gmail.com

**Professor in the Department of Electrical and Computer engineering, Brigham Young University, Provo, USA, beard@byu.edu

On the other hand, local path planning is executed in real-time during flight. The basic idea is to first sense the obstacles in the environment and then determine a collision-free path [1]. Local path planning algorithms require sensors to detect obstacles. Among the suite of possible sensors, a video camera is cheap and lightweight and fits the physical requirements of MAVs [1]. Since the camera measurements are obtained in the body frame, it is most natural to create maps and to plan paths directly in the local-level frame of the MAV. References [8]–[11] develop vision-based local-level frame mapping and path planning algorithms that create polar and cylindrical maps and plan paths using time-to-collision (TTC) and bearing measurements obtained by a camera directly without transforming to the inertial frame. However, if we use a single camera to detect obstacles, the TTC measurements are usually inaccurate, which motivates the use of bearing-only measurements obtained by the camera to estimate both the TTC and bearing. Our previous work in [12] develops an observability-based planning technique for MAVs, where the TTC and bearing are estimated using bearing-only measurement, and where a two dimensional planning algorithm is developed to minimize the uncertainties of the state estimates while simultaneously avoiding collisions. However, in [12], the obstacle initialization problem was not addressed and the behavior of the planning algorithm was not carefully analyzed.

Feature initialization is an important problem caused by bearing-only camera. Since the camera only provides the bearing to a feature, the TTC estimate for the feature is uncertain when it is initially observed or when the feature exhibits low parallax during motion of the platform. The uncertainties are not well represented by a Gaussian distribution in the context of an extended Kalman Filter (EKF) [13]. There have been methods presented for addressing the feature initialization problem in the Simultaneously Localization and Mapping (SLAM) community. The methods are classified into delayed and undelayed initialization.

Delayed initialization methods consider the new observed features separately from the map and accumulate depth information over several video frames to reduce depth uncertainty before adding the new features to the map [14]–[16]. However, the drawback of using these methods for collision avoidance is that the new observed obstacles do not contribute to the path generation until they are added to the map. Reference [13] develops an undelayed feature initialization method that can handle the initialization of features at all depths within the

standard EKF framework using direct parametrization of inverse depth relative to the camera position from which a feature was first observed. The inverse depth parametrization represents a feature by a six-state vector, which is more computationally expensive. Once the depth estimate is accurate enough, the inverse depth parametrization is converted to Euclidean XYZ form to speed up the computation.

This paper explores a vision-based local-level frame mapping and planning technique for MAVs. Using bearing-only measurements obtained by a monocular camera, we employ an EKF to estimate the inverse TTC, azimuth, and elevation angles to near-by obstacles, and then construct a map in local-level spherical coordinates. The spherical map is parameterized using the inverse TTC, azimuth, and elevation, which is independent of the ground speed of the MAV and which allows the obstacle initialization problem to be addressed explicitly. In addition, compared to using a switching strategy between the inverse depth parametrization and Euclidean XYZ representation, parameterizing the map only using the inverse TTC, azimuth, and elevation enhances the computational efficiency. We perform the observability analysis of the state estimation process from bearing-only measurements and find the conditions for the observability of the system. Based on the conditions, we design the planning algorithm that minimizes the uncertainties of the state estimates while simultaneously avoiding collisions with obstacles. We analyze the behavior of the planning algorithm and describe the characteristics of the environment in which the algorithm guarantees collision-free paths for the MAV.

The paper is organized as follows. Section II describes the vision-based spherical mapping in the local-level frame using the inverse TTC, azimuth, and elevation. A nonlinear observability analysis of the system is also presented. In Section III, the planning algorithm is designed based on the observability conditions. Section IV analyzes the behavior of the planning algorithm. Section V presents numerical results demonstrating the effectiveness of the algorithm.

## II. Vision-based local-level frame mapping in spherical coordinates

In this section we will build a map using the inverse TTC to obstacles in the local-level frame of the MAV. The map is constructed in spherical coordinates by estimating the inverse TTC, azimuth, and elevation to obstacles. We then perform a nonlinear observability analysis of the state estimation problem using bearing-only measurements, and find the conditions for observability of the system.

### A. Estimates of inverse TTC, azimuth, and elevation

Since the obstacle map is constructed in the local-level frame, the equation of motion of each obstacle relative to the MAV needs to be derived. Throughout the paper we will assume zero wind conditions. Let $V$ represent the ground speed of the MAV and let $\psi$ and $\theta$ represent the heading and pitch angles respectively. Figure 1 shows the motion of the $i^{th}$ obstacle relative to the MAV in the local-level frame, where $O^i$ represents the obstacle, and $\tau^i$, $\eta^i$ and $\xi^i$ are the inverse TTC, azimuth, and elevation to the obstacle. Based on

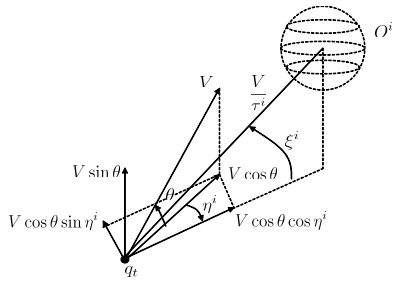


Fig. 1. This figure shows the motion of the $i^{th}$ obstacle relative to the MAV. The current MAV configuration is $q_t$. The obstacle is represented by $O^i$. The pitch angle is represented by $\theta$. The inverse TTC, azimuth, and elevation to the obstacle are represented by $\tau^i$, $\eta^i$ and $\xi^i$. The ground speed is represented by $V$.

Fig. 1, the equation of motion of the obstacle relative to the MAV in terms of the inverse TTC, azimuth, and elevation is given by

$$\begin{aligned}\dot{\mathbf{x}}^i &= \mathbf{f}(\mathbf{x}^i,\mathbf{u})+\mathbf{w}^i \\ &= \begin{bmatrix} (\tau^i)^2\cos\theta\cos\eta^i\cos\xi^i+(\tau^i)^2\sin\theta\sin\xi^i \\ \tau^i\frac{\cos\theta\sin\eta^i}{\cos\xi^i}-\dot{\psi} \\ \tau^i\cos\theta\cos\eta^i\sin\xi^i-\tau^i\sin\theta\cos\xi^i \end{bmatrix}+\mathbf{w}^i, \end{aligned} \quad (1)$$

where we have assumed coordinated turn conditions $\dot{\psi}=\frac{g}{V}\tan\phi$, and where $g$ is the gravity constant and $\phi$ is the roll angle of the MAV, $\mathbf{x}^i=[\tau^i,\eta^i,\xi^i]^\top$ is the state, $\mathbf{u}=[\phi,\theta]^\top$ is the control input, and the process noise $\mathbf{w}^i$ is a Gaussian random vector with zero mean and covariance matrix $\mathbf{Q}^i$.

Since the camera directly measures the azimuth and elevation angles, the measurement at time step $k$ is given by

$$\mathbf{z}_k^i=\mathbf{h}(\mathbf{x}_k^i)+\mathbf{v}_k^i=\begin{bmatrix}\eta_k^i\\ \xi_k^i\end{bmatrix}+\mathbf{v}_k^i, \quad (2)$$

where the measurement noise $\mathbf{v}_k^i$ is a Gaussian random vector with zero mean and covariance matrix $\mathbf{R}_k^i$. Based on Eqs. (1) and (2), the inverse TTC, azimuth, and elevation are estimated using the standard continuous-discrete time EKF algorithm [17].

When an obstacle is observed for the first time, we initialize the azimuth and elevation using the measurement data. The uncertainties of the initial inverse TTC to the obstacle can be well approximated by a Gaussian distribution with the mean $\tau_0$ and the standard deviation $\sigma_{\tau_0}$ [13]. The values for $\tau_0$ and $\sigma_{\tau_0}$ are set empirically such that the 95% confidence region spans a range of the TTC from close to the camera up to infinity. Let $\mathbf{z}_k^i$ represent the measurement for the new observed obstacle and let $\mathbf{R}_k^i$ represent the covariance matrix of measurement noise for that obstacle. The state for the obstacle is given by $[\tau_0,\mathbf{z}_k^{i\top}]^\top$ and the error covariance matrix is given by $\begin{bmatrix}\sigma_{\tau_0}^2 & \mathbf{0}\\ \mathbf{0} & \mathbf{R}_k^i\end{bmatrix}$.

The local-level frame map only contains obstacles with the inverse TTC greater than a certain threshold $\tau^l$ and with the

absolute value of the azimuth and elevation angles less than $\frac{\pi}{2}$. When an obstacle disappears from the local-level frame map, it will be removed from the map.

### B. Local-level frame mapping in spherical coordinates

We build a map directly in the local-level frame instead of inertial frame. Accordingly, we save the computational expense, and the errors associated with transforming the camera data from the local-level frame to the inertial frame, at the expense of updating the map using body motion. We construct maps in spherical coordinates, which are more compatible with bearing information obtained by the camera, allowing the data to be processed more efficiently. The maps are constructed using the inverse TTC, azimuth, and elevation, as shown in Fig. 2. The origin of the map is the current location of the MAV. The blue dots are a numerical representation of 95% uncertainty region Gaussian in the inverse TTC for each obstacle.

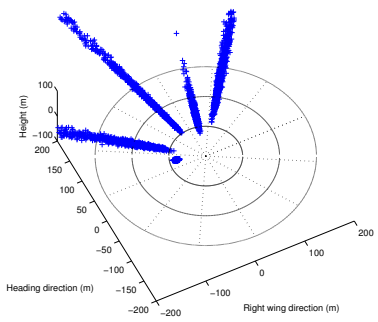


Fig. 2. This figure shows the local-level frame map in spherical coordinates. The origin of the map is the current location of the MAV. The blue dots are a numerical representation of 95% uncertainty region Gaussian in the inverse TTC for each obstacle.

### C. Observability analysis

We use the EKF to estimate the inverse TTC, azimuth, and elevation to obstacles using bearing-only measurements. To bound the error covariance computed by the EKF, the system should be observable. We use the nonlinear observability theory developed in [18], which states that the observability is achieved when a system satisfies the nonlinear observability rank condition. Accordingly, we analyze the observability of the system for the $i^{th}$ obstacle given by Eqs. (1) and (2) by computing the rank of the observability matrix. For an angle $\alpha$, define $c_\alpha \triangleq \cos\alpha$ and $s_\alpha \triangleq \sin\alpha$. The observability matrix is computed using Lie derivatives as described in [18]. The $0^{th}$ order Lie derivative is

$$L^0_{\mathbf{f}}(\mathbf{h}) = \begin{bmatrix} \eta^i \\ \xi^i \end{bmatrix}. \tag{3}$$

The $1^{st}$ order Lie derivative is given by

$$L^1_{\mathbf{f}}(\mathbf{h}) = \begin{bmatrix} \tau^i \frac{c_\theta s_{\eta^i}}{c_{\xi^i}} - \dot{\psi} \\ \tau^i c_\theta c_{\eta^i} s_{\xi^i} - \tau^i s_\theta c_{\xi^i} \end{bmatrix}. \tag{4}$$

The $2^{nd}$ order Lie derivative is given by

$$L^2_{\mathbf{f}}(\mathbf{h}) = \begin{bmatrix} \frac{2(\tau^i)^2 c^2_\theta s_{\eta^i} c_{\eta^i}}{c^2_{\xi^i}} - \dot{\psi}\frac{\tau^i c_\theta c_{\eta^i}}{c_{\xi^i}} \\ 2(\tau^i)^2 s_\theta c_\theta c_{\eta^i} s^2_{\xi^i} - 2(\tau^i)^2 s_\theta c_\theta c_{\eta^i} c^2_{\xi^i} \\ +2(\tau^i)^2 c^2_\theta c^2_{\eta^i} c_{\xi^i} s_{\xi^i} - 2(\tau^i)^2 s^2_\theta c_{\xi^i} s_{\xi^i} \\ -\frac{(\tau^i)^2 c^2_\theta s^2_{\eta^i} s_{\xi^i}}{c_{\xi^i}} - \tau^i c_\theta s_{\eta^i} s_{\xi^i} \dot{\psi} \end{bmatrix}. \tag{5}$$

The observability matrix is computed as

$$\mathbf{O}^i = \begin{bmatrix} 0 & 1 & 0 \\ 0 & 0 & 1 \\ \frac{c\theta s_{\eta^i}}{c_{\xi^i}} & \frac{\tau^i c\theta c_{\eta^i}}{c_{\xi^i}} & \frac{\tau^i c_{\theta s_{\eta^i} s_{\xi^i}}}{c^2_{\xi^i}} \\ \mathbf{O}^i_{41} & \mathbf{O}^i_{42} & \mathbf{O}^i_{43} \\ \mathbf{O}^i_{51} & \mathbf{O}^i_{52} & \mathbf{O}^i_{53} \\ \mathbf{O}^i_{61} & \mathbf{O}^i_{62} & \mathbf{O}^i_{63} \end{bmatrix}, \tag{6}$$

where

$$\begin{aligned}
\mathbf{O}^i_{41} &= c_\theta c_{\eta^i} s_{\xi i} - s_\theta c_{\xi i}, \\
\mathbf{O}^i_{42} &= -\tau^i c_\theta s_{\eta^i} s_{\xi i}, \\
\mathbf{O}^i_{43} &= \tau^i c_\theta c_{\eta^i} c_{\xi i} + \tau^i s_\theta s_{\xi i}, \\
\mathbf{O}^i_{51} &= \frac{4\tau^i c^2_\theta s_{\eta^i} c_{\eta^i}}{c^2_{\xi i}} - \frac{\dot{\psi} c_\theta c_{\eta^i}}{c_{\xi i}}, \\
\mathbf{O}^i_{52} &= \frac{2(\tau^i)^2 c^2_\theta c^2_{\eta^i}}{c^2_{\xi i}} - \frac{2(\tau^i)^2 c^2_\theta s^2_{\eta^i}}{c^2_{\xi i}} + \frac{\dot{\psi}\tau^i c_\theta s_{\eta^i}}{c_{\xi i}}, \\
\mathbf{O}^i_{53} &= \frac{2(\tau^i)^2 c^2_\theta s_{\xi i} s_{\eta^i} c_{\eta^i}}{c^3_{\xi i}} - \frac{\dot{\psi}\tau^i c_\theta c_{\eta^i} s_{\xi i}}{c^2_{\xi i}}, \\
\mathbf{O}^i_{61} &= 4\tau^i s_\theta c_\theta c_{\eta^i} s^2_{\xi i} - 4\tau^i s_\theta c_\theta c_{\eta^i} c^2_{\xi i} \\
&\quad +4\tau^i c^2_\theta c^2_{\eta^i} c_{\xi i} s_{\xi i} - 4\tau^i s^2_\theta c_{\xi i} s_{\xi i} \\
&\quad -\frac{2\tau^i c^2_\theta s^2_{\eta^i} s_{\xi i}}{c_{\xi i}} - c_\theta s_{\eta^i} s_{\xi i} \dot{\psi}, \\
\mathbf{O}^i_{62} &= -2(\tau^i)^2 s_\theta c_\theta s_{\eta^i} s^2_{\xi i} + 2(\tau^i)^2 s_\theta c_\theta s_{\eta^i} c^2_{\xi i} \\
&\quad -4(\tau^i)^2 c^2_\theta c_{\eta^i} s_{\eta^i} c_{\xi i} s_{\xi i} \\
&\quad -\frac{2(\tau^i)^2 c^2_\theta s_{\eta^i} c_{\eta^i} s_{\xi i}}{c_{\xi i}} - \tau^i c_\theta c_{\eta^i} s_{\xi i} \dot{\psi}, \\
\mathbf{O}^i_{63} &= 4\tau^i s_\theta c_\theta c_{\eta^i} s_{\xi i} c_{\xi i} + 4(\tau^i)^2 s_\theta c_\theta c_{\eta^i} c_{\xi i} s_{\xi i} \\
&\quad +2(\tau^i)^2 c^2_\theta c^2_{\eta^i} c^2_{\xi i} - 2(\tau^i)^2 c^2_\theta c^2_{\eta^i} s^2_{\xi i} \\
&\quad +2(\tau^i)^2 s^2_\theta s^2_{\xi i} - 2(\tau^i)^2 s^2_\theta c^2_{\xi i} \\
&\quad -\tau^i c_\theta s_{\eta^i} c_{\xi i} \dot{\psi} - \frac{(\tau^i)^2 c^2_\theta s^2_{\eta^i}}{c^2_{\xi i}}.
\end{aligned}$$

Based on the observability matrix, Lemma 1 gives the conditions under which the system for the $i^{th}$ obstacle is observable.

*Lemma 1:* The $i^{th}$ obstacle, whose motion is given by Eqs. (1) and (2), is locally observable at time $t$ if and only if at least one of the following three conditions is satisfied (a) $\eta^i(t) \neq 0$, (b) $\xi^i(t) \neq \theta(t)$, and (c) $\phi(t) \neq 0$, where $\eta^i(t)$ and

$\xi^i(t)$ are the azimuth and elevation angles to the obstacle, and $\phi(t)$ and $\theta(t)$ are the roll and pitch angles of the MAV.

*Proof:* The observability matrix given by Eq. (6), has rank two if and only if all elements in the first column are zero. Accordingly, the $i^{th}$ obstacle, whose motion is given by Eqs. (1) and (2), is not locally observable if and only if all elements in the first column are zero. For $\mathbf{O}^i_{31}$ to equal zero at time $t$, it must be that $\eta^i(t) = 0$. For $\mathbf{O}^i_{41}$ to equal zero at time $t$, it must be that $\xi^i(t) = \theta(t)$. For $\mathbf{O}^i_{51}$ to equal zero at time $t$, it must be that $\dot{\psi} = \frac{g}{V}\tan\phi = 0$, which implies $\phi(t) = 0$. Substituting $\eta^i(t) = 0$, $\xi^i(t) = \theta(t)$ and $\phi(t) = 0$ into $\mathbf{O}^i_{61}$ also leads to $\mathbf{O}^i_{61} = 0$. Therefore, the system is not locally observable at time $t$ if and only if all three conditions of (a) $\eta^i(t) = 0$, (b) $\xi^i(t) = \theta(t)$, and (c) $\phi(t) = 0$ are satisfied. ■

The conditions in Lemma 1 show that the system is locally observable when the MAV does not directly fly toward the obstacle. When the MAV is not flying directly at the obstacle, parallax can be used to estimate time-to-collision and the system is always locally observable, which implies that the system is observable [18].

## III. Path planning in the local-level frame

The convergence and boundedness of the EKF are achieved when the system is fully observable [19]. Bounds on the EKF error covariance $\mathbf{P}^i$ for the $i^{th}$ obstacle are related to the observability of the system given by Lemma 2 as shown in [19].

*Lemma 2 ( [19]):* Suppose that there exist positive real scalars $\alpha_1,\ \alpha_2,\ \beta_1,\ \beta_2$ such that $\beta_1\mathbf{I} \leq \mathbf{O}^{i\top}\mathbf{O}^i \leq \beta_2\mathbf{I}$ and $\alpha_2\mathbf{I} \geq \mathbf{C}^i\mathbf{C}^{i\top} \geq \alpha_1\mathbf{I}$ then,

$$\left(\frac{1}{\beta_2 + \frac{1}{\alpha_1}}\right)\mathbf{I} \leq \mathbf{P}^i_k \leq \left(\alpha_2 + \frac{1}{\beta_1}\right)\mathbf{I}, \tag{7}$$

where $\mathbf{C}^i$ is the controllability matrix.

We design the path planning algorithm that minimizes the uncertainties of the inverse TTC, azimuth, and elevation estimates while causing the MAV to avoid collisions. Based on Lemma 2, we can see that the minimum eigenvalue of the matrix $\mathbf{O}^{i\top}\mathbf{O}^i$ determines the upper bound on the error covariance. To minimize the upper bound on the error covariance, the minimum eigenvalue should be maximized, which is equivalent to minimizing the inverse of the minimum eigenvalue. When the system is unobservable, the rank of the observability matrix is two and the inverse of the minimum eigenvalue is infinite. When the system is observable, the rank of the observability matrix is three and the inverse is finite. Minimizing the inverse of the minimum eigenvalue ensures that the observability conditions given by Lemma 1 are satisfied. This implies that the minimization of the inverse of the minimum eigenvalue will minimize the upper bound of the error covariance as well as steer the MAV away from the obstacle. Therefore, the minimization of uncertainties and obstacle avoidance are complementary.

Let $\tau^g_t$, $\eta^g_t$ and $\xi^g_t$ represent the inverse TTC, azimuth, and elevation to the goal configuration at time $t$, and let $\mathbf{x}^g_t = [\tau^g_t, \eta^g_t, \xi^g_t]^\top$. Suppose there exist $n$ obstacles in the local map. Let $\mathbf{x}^i_t = [\tau^i_t, \eta^i_t, \xi^i_t]^\top$ represent the state for the $i^{th}$ obstacle. Let $\nu_t = [\mathbf{x}^{g\top}_t, \mathbf{x}^{1\top}_t, \cdots, \mathbf{x}^{n\top}_t]^\top$. Define the utility function $S : \mathbb{R}^{3n+3} \to \mathbb{R}$ as

$$S(\nu_t) = \frac{a_1}{(\tau^g_t)^2} + a_2(\eta^g_t)^2 + a_3(\xi^g_t)^2 + \sum_{i=1}^{n}\frac{b_i}{\lambda_{min}(\mathbf{O}^{i\top}\mathbf{O}^i)}, \tag{8}$$

where $a_1,\ a_2,\ a_3,\ b_i,\ i = 1,\cdots,n$ are positive weights and $\lambda_{min}(\mathbf{O}^{i\top}\mathbf{O}^i)$ is the minimum eigenvalue of the matrix $\mathbf{O}^{i\top}\mathbf{O}^i$. The first three terms penalize the cost for goal reaching. The fourth term penalizes the weighted sum of the inverse of the minimum eigenvalue for all obstacles. By minimizing the fourth term, the algorithm minimizes the uncertainties in the inverse TTC, azimuth, and elevation estimates and also steers the MAV around the obstacles. We use the look-ahead policy over the horizon $T$ that minimizes the cost function

$$J = \int_t^{t+T} S(\nu_\rho)d\rho, \tag{9}$$

subject to the constraints

$$\begin{aligned} &\dot{\mathbf{x}}^g_\rho = \mathbf{f}(\mathbf{x}^g_\rho, \mathbf{u}_\rho),\\ &\dot{\mathbf{x}}^i_\rho = \mathbf{f}(\mathbf{x}^i_\rho, \mathbf{u}_\rho),\ i = 1,\cdots,n,\\ &|\phi_\rho| \leq \phi_{\max},\\ &|\theta_\rho| \leq \theta_{\max}. \end{aligned} \tag{10}$$

We solve the constrained optimization problem using the nonlinear optimization function fmincon in MATLAB [20].

## IV. Analysis

In this section, we analyze the behavior of the planning algorithm and describe the characteristics of the environments in which the algorithm guarantees collision-free paths for the MAV. We focus our analysis on environments with spherical obstacles with known locations. For the sake of saving space, we will not provide the proofs of the theoretical results presented in this section. The proofs will be given in a coming journal article.

For avoiding spherical obstacles, the optimization needs additional constraints

$$\frac{V}{\tau^i_\rho} \geq R^i_s,\ i = 1,\cdots,n,\ \forall\rho \in [t, t+T], \tag{11}$$

where $R^i_s$ is the radius of the $i^{th}$ obstacle. To guarantee collision avoidance, it is necessary to establish a minimum turn away distance $d^i_{\min}$ from each obstacle. The minimum turn away distance is evaluated at the horizontal plane of the MAV's center of mass. Let $\phi_{\max}$ represent the maximum roll angle of the MAV and let $\theta_{\max}$ represent the maximum pitch angle. The minimum turning radius of the MAV is then given by [21]

$$r_{mt} = \frac{V^2\cos\theta_{\max}}{g\tan\phi_{\max}}. \tag{12}$$

Lemma 3 shows the minimum turn away distance for the MAV to avoid a spherical obstacle $O^i$ with the radius $R^i_s$ using the planning algorithm.

*Lemma 3:* Using the planning algorithm which minimizes the cost function (9) subject to the constraints (10) and (11), avoidance of a collision with a spherical obstacle $O^i$ with the radius $R_s^i$ is guaranteed if the turn away distance from the obstacle satisfies $d > d_{\min}^i = \sqrt{(R_s^i + r_{mt})^2 - r_{mt}^2} - R_s^i$.

For the environments with multiple spherical obstacles, we specify the conditions under which the planning algorithm is guaranteed to generate collision-free paths for the MAV. Let $\mathscr{C}$ represent the configuration space. For two configurations $q_1 = [q_{1n}, q_{1e}, q_{1d}, q_{1\psi}, q_{1\theta}]^\top \in \mathscr{C}$ and $q_2 = [q_{2n}, q_{2e}, q_{2d}, q_{2\psi}, q_{2\theta}]^\top \in \mathscr{C}$, where $q_{in}$, $q_{ie}$, and $q_{id}$, $i = 1,2$, represent North, East, and Down coordinates, and $q_{i\psi}$ and $q_{i\theta}$, $i = 1,2$, represent the heading and pitch angles, define the two dimensional distance between $q_1$ and $q_2$ projected on $x$-$y$ plane of the inertial frame

$$\|q_1 - q_2\|_{2D} \triangleq \sqrt{(q_{1n} - q_{2n})^2 + (q_{1e} - q_{2e})^2}. \tag{13}$$

Let $q_0$ represent the initial MAV configuration and let $q_{O^i} = [q_{O^i n}, q_{O^i e}, q_{O^i d}, q_{O^i \psi}, q_{O^i \theta}]^\top$ represent the configuration of the $i^{th}$ obstacle's center. Let $d_{q_0}^i = \min_{q \in \partial O^i} \|q_0 - q\|_{2D}$ represent the two dimensional distance between $q_0$ and the boundary of the $i^{th}$ obstacle. Let $d^{ij} = \min_{p_i \in \partial O^i, p_j \in \partial O^j} \|p_i - p_j\|_{2D}$ represent the shortest two dimensional distance between the points along the boundaries of the $i^{th}$ obstacle and the $j^{th}$ obstacle. Let $\mathscr{I}$ represent the index set of obstacles and let $D \triangleq \{(i,j) \in \mathscr{I} \times \mathscr{I} : |q_{O^i d} - q_{O^j d}| \leq (R_s^i + R_s^j)\}$ represent the set of obstacle pairs in which the altitude difference between each two obstacles is no greater than the sum of their radii. We introduce the notion of local sparseness as Definition 1.

*Definition 1:* An environment is said to be *locally sparse* if $d^{ij} > \max\{d_{\min}^i, d_{\min}^j\}$, $\forall (i,j) \in D$.

The local sparseness property means that each two obstacles in the environment with the altitude difference between them less than the sum of their radii are separated enough from each other such that the distance between them is greater than the maximum of their minimum turn away distances.

*Theorem 1:* If the environment is locally sparse and the initial MAV configuration satisfies $d_{q_0}^i > d_{\min}^i$, $\forall i \in \mathscr{I}$, then the planning algorithm, which minimizes the cost function (9) subject to the constraints given by (10) and (11), is guaranteed that the MAV will avoid all the obstacles for all time $t$.

We assume that the environment is locally sparse in order to provide a theoretical guarantee for collision avoidance behavior of the planning algorithm. The assumptions are only sufficient conditions for collision avoidance, which means there may exist environments that are not locally sparse but where the planning algorithm can still maneuver the MAV without causing collisions.

## V. Numerical results

The feasibility of the observability-based planning algorithm was tested using a simulation environment developed in MATLAB/SIMULINK, as shown in the subfigures on the right in Fig. 3. The simulator uses a six degree of freedom model of the aircraft, where a North-East-Down (NED) coordinate system is used. The covariance matrix of the process noise for each obstacle was $\mathbf{Q}^i = \begin{bmatrix} 0.00001 & 0 & 0 \\ 0 & 0.0001 & 0 \\ 0 & 0 & 0.0001 \end{bmatrix}$ and the covariance matrix of the measurement noise was $\mathbf{R}^i = \begin{bmatrix} 0.0012 & 0 \\ 0 & 0.0012 \end{bmatrix}$. The values for the initial inverse TTC and its standard deviation were set at $\tau_0 = 0.06$ and $\sigma_{\tau_0} = 0.03$. The ground speed was $V = 13$ m/s. The maximum roll and flight path angles for the MAV were 30° and 15° respectively. The weights were selected as $a_i = 1, \forall i = 1, \cdots, 3$, and $b_i = 0.04, \forall i = 1, \cdots, n$. The look-ahead policy over the horizon 3.6 seconds was used.

The MAV was commanded to maneuver through twenty-five spherical obstacles between waypoint **S** (0,100,-20) and waypoint **E** (600,700,-100). Figure 3 shows the evolution of the maps using the inverse TTC parametrization in the local-level frame and the update of the actual paths followed by the MAV in the inertial frame. Subfigures on the left show the local-level frame maps in spherical coordinates. Subfigures on the right show the actual paths. Based on the figure, when the obstacle is first observed, the 95% acceptance region of the inverse TTC includes $\tau = 0$. Accordingly, the uncertainties in the inverse TTC map to the infinity depth. As time progresses, parallax reduces the uncertainties which become progressively smaller, causing the uncertainties in the depth to be reduced. Figure 4 shows the tracking error and $\pm 2\sigma$ bounds for the inverse TTC, azimuth, and elevation to the obstacle with $x$ and $y$ coordinates at $(150, 250)$.

## VI. Conclusion

This paper presents a vision-based local-level frame mapping and planning technique for MAVs. To explicitly address the obstacle initialization problem, we construct the local-level frame maps in spherical coordinates using the inverse TTC, azimuth, and elevation to obstacles. Using bearing-only measurements, we employ an EKF to estimate the inverse TTC, azimuth, and elevation, and perform an observability analysis of the state estimation to find the conditions under which the system is observable. Based on the conditions, we design a planning algorithm that minimizes the estimation uncertainties while simultaneously avoiding collisions. We describe the characteristics of the environments in which the planning algorithm guarantees collision-free paths for the MAVs.


## Acknowledgment

This research was supported by OSD and AFRL under contract no. FA 8650-08-C-1411 to SET, Inc. and Brigham Young University.


## References


[1] B. Call, "Obstacle avoidance for Unmanned Air Vehicles using computer vision," Master's thesis, Brigham Young University, December, 2006.

[2] A. Curtis, "Path planning for Unmanned Air and Ground Vehicles in urban environments," Master's thesis, Brigham Young University, 2008.

[3] E. Frazzoli, M. Dahleh, and E. Feron, "Real-time motion planning for agile autonomous vehicles," *Journal of Guidance, Control and Dynamics*, vol. 25, pp. 116–129, Jan.-Feb. 2002.

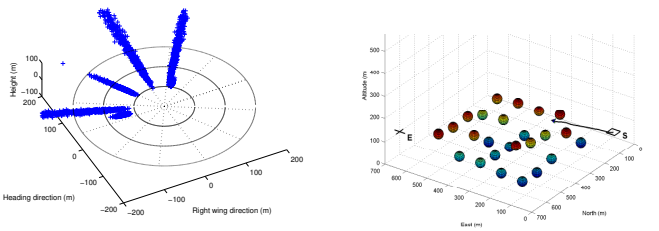


(a) $t = 12$ s

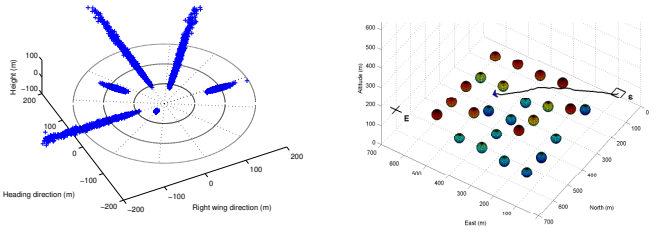


(b) $t = 35$ s

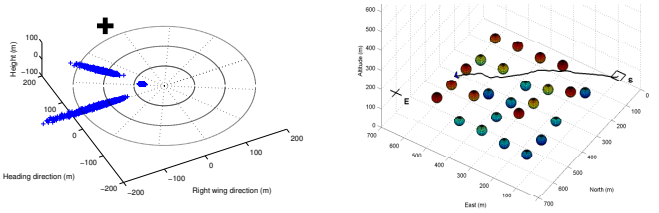


(c) $t = 57$ s

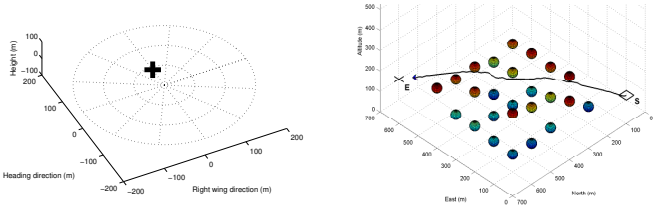


(d) $t = 70$ s

Fig. 3. This figure shows the evolution of the maps using the inverse TTC parametrization in the local-level frame and the update of the actual paths followed by the MAV in the inertial frame.

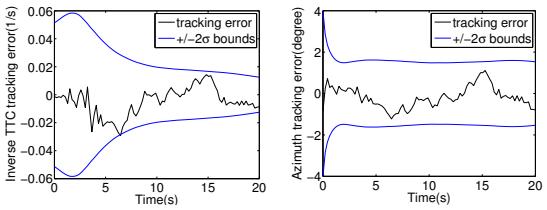


(a) Inverse TTC tracking error (b) Azimuth tracking error

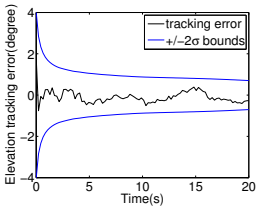


(c) Elevation tracking error

Fig. 4. This figure shows the tracking error and $\pm 2\sigma$ bounds for the inverse TTC, azimuth, and elevation to the obstacle with x and y coordinates at $(150, 250)$.


[4] Y. Watanabe, E. Johnson, and A. Calise, "Vision-based approach to obstacle avoidance," in *Proceedings of the AIAA Guidance, Navigation, and Control Conference and Exhibit*, August 2005.

[5] A. Pongpunwattana and R. Rysdyk, "Real-time planning for multiple autonomous vehicles in dynamics uncertain environments," *AIAA Journal of Aerospace Computing, Information, and Communication*, vol. 1, pp. 580–604, December 2004.

[6] K. Sedighi, K. Ashenayi, R. Wainwright, and H. Tai, "Autonomous local path planning for a mobile robot using a genetic algorithm," *Congress on Evolutionary Computation*, vol. 2, pp. 1338–1345, June 2004.

[7] J. Latombe, *Robot Motion Planning*. Kluwer Academic Publishers, Boston, MA, 1991.

[8] H. Yu, R. Beard, and J. Byrne, "Vision-based local multi-resolution mapping and path planning for Miniature Air Vehicles," in *Proceedings of American Control Conference*, June 10-12 2009.

[9] ——, "Vision-based local multi-resolution path planning and obstacle avoidance for Micro Air Vehicles," in *Proceedings of the AIAA Guidance, Navigation and Control Conference*, August 10 2009.

[10] ——, "Vision-based navigation frame mapping and planning for collision avoidance for Miniature Air Vehicles," *Special Issue on Aerial Robotics, Control Engineering Practice*, vol. 18, no. 7, pp. 824–836, July 2010.

[11] H. Yu and R. Beard, "Vision-based three dimensional navigation frame mapping and planning for collision avoidance for Micro Air Vehicles," in *Proceedings of AIAA Guidance, Navigation, and Control Conference*, August 2-5 2010.

[12] H. Yu, R. Sharma, R. Beard, and C. Taylor, "Observability-based local path planning and collision avoidance for Micro Air Vehicles using bearing-only measurements," in *Proceedings of IEEE American Control Conference*, 2011(to appear).

[13] J. Civera, A. Davision, and J. Montiel, "Inverse depth parametrization for monocular SLAM," *IEEE Transactions on Robotics*, vol. 24, pp. 932–945, Oct. 2008.

[14] M. Bryson and S. Sukkarieh, "Bearing-only SLAM for an airborne vehicle," in *Australian Conference on Robotics and Automation (ACRA' 05)*, Sidney, 2005.

[15] A. Davision, "Real-time simultaneous localization and mapping with a single camera," in *In Proc. International Conference on Computer Vision*, 2003.

[16] J. H. Kim and S. Sukkarieh, "Airborne simultaneous localisation and map building," in *In Proceedings of the IEEE International Conference on Robotics and Automation*, 2003, pp. 406–411.

[17] F. Lewis, *Optimal Estimation: With An Introduction To Stochastic Control Theory*. New York: Wiley, 1986.

[18] R. Hermann and A. Krener, "Nonlinear controllability and observability," *IEEE Transaction on Automatic Control*, vol. 22, no. 5, pp. 728–740, Oct 1977.

[19] Y. Song and J. W. Grizzle, "The extended Kalman Filter as a local asymptotic observer for discrete-time nonlinear system," *Journal of Mathemetical Systems, Estimation, and Control*, vol. 5, pp. 59–78, 1995.

[20] *MathWorks, Optimization Toolbox, http://www.mathworks.com/.*

[21] R. W. Beard and T. W. McLain, *Small Unmanned Aircraft: Theory and Practice*. Princeton University Press, 2011 (to appear).